Available online at www.sciencedirect.com
ScienceDirect
International Journal of Heat and Mass Transfer 50 (2007) 3583–3598
International Journal of HEAT and MASS TRANSFER
www.elsevier.com/locate/ijhmt

Hopf bifurcation in mixed convection flow inside a rectangular cavity

Y. Sunil Prasad [1], Manab Kumar Das *

Department of Mechanical Engineering, Indian Institute of Technology Guwahati, North Guwahati, Guwahati 781039, Assam, India

Received 8 February 2006; received in revised form 12 July 2006
Available online 26 March 2007

Abstract

In the present paper, a study of mixed convection inside a rectangular cavity has been carried out. The Reynolds number (Re) has been kept at 100 while the Grashof number (Gr) has been varied between 0, $\pm 10^4$, $\pm 10^6$ and aspect ratio (AR) (height/width) = 0.5, 1 and 2 keeping the Prandtl number (Pr) = 1. The two vertical walls are maintained at cold temperature $T = 0$. In one case the top-moving wall is maintained at hot $T = 1$ and the bottom is cold $T = 0$ and in the other case, the top is cold $T = 0$ and the bottom is hot $T = 1$. The integral form of the governing equations are solved numerically using finite-volume method. SIMPLE algorithm with higher-order upwinding scheme is used. Results are presented in the form of local and average Nusselt number distribution for the range of Grashof number and aspect ratio. The streamlines and isothermal lines are also presented. A Hopf bifurcation has been observed at $Gr = -10^5$ for aspect ratio 2. A periodic oscillation of the total kinetic energy (TKE) occurs with the period 4.368 non-dimensional time.

Keywords: Mixed convection; Numerical simulation; Hopf bifurcation; Rectangular cavity; Finite volume method

1. Introduction

Heat transfer in flows in which the influence of forced convection and natural convection are of comparable magnitude (commonly referred to as mixed-convection flows) occurs frequently in engineering situations. The applications include solar collector, nuclear reactor, lakes and reservoirs, crystal growth etc. Analysis of a mixed convection flow usually requires an understanding of the two limiting regimes. The mixed convection transport is complex due to the interaction of buoyancy force with the shear force.

A review shows that there are two kinds of studies, the first one is concerned with the horizontal top or bottom wall sliding lid-driven cavities, in which firstly the top wall has a constant velocity U and temperature T_1. The remaining walls are stationary and temperature T_0 [1]. They have considered variation of the $Gr = 0$, $\pm 10^4$, $\pm 10^6$ and aspect ratio (height/width) $= \frac{1}{2}$, 1 and 2 keeping the Re constant at 100 and $Pr = 1$. They reported that the buoyancy has a marked influence for the larger aspect ratios when $Gr = \pm 10^4$ and the dominance of buoyancy for all aspect ratios when the $Gr = \pm 10^6$. In other case, the top wall is moving at a constant velocity U and maintained at a temperature T_1. The bottom wall is stationary at T_0. The left and right vertical walls are adiabatic [2]. The study has been carried out for $Re = 3000$ whereas Ra varied up to 10^6. As $Gr/Re^2 \le 1$, the effect of convection is more and the isotherm shows a thermally non-stratified nature similar to a driven-cavity flow. When it is increased beyond 1, much of the middle and bottom portions of the cavity has horizontal temperature distributions. The Nusselt number at the top shows that the heat transfer intensifies as $Gr/Re^2 \ll 1$. The mixed convection problem in a similar geometry and boundary conditions have been solved by Khanafer and Chamkha [3]. However, they have considered the effect of porous medium while solving the mixed convection problem. In another study, the top wall is moving at a constant velocity U and is cooled at temperature T_0. The lower wall is heated and maintained at T_1. In the experiments conducted by Prasad and Koseff [4], the Re

* Corresponding author. Tel.: +91 361 2582655; fax: +91 361 2690762. *E-mail address:* manab@iitg.ernet.in (M.K. Das).
[1] Present address: Assistant Engineer, Hindustan Aeronautics Limited, P.B. No. 7835, Sunabeda 763002, Koraput District, Orissa, India.

0017-9310/$ - see front matter
doi:10.1016/j.ijheatmasstransfer.2006.11.048

Nomenclature

AR	aspect ratio $(= H/L)$
dt	time step
g	gravitational acceleration (m/s^2)
Gr	Grashof number $(= g\beta\Delta TL^3/\nu^2)$
H	height of the enclosure (m)
L	length of the enclosure (m)
nx, ny	number of grids in x- and y-directions respectively
Nu	Nusselt number
p	dimensionless pressure
Pr	Prandtl number $(= \nu/\alpha)$
Ra	Rayleigh number $(= g\beta\Delta TL^3/\nu\alpha)$
Re	Reynolds number $(= UL/\nu)$
Ri	Richardson number $(= Gr/Re^2)$
t	nondimensional time
T	dimensionless temperature
ΔT	differential temperature, dimensionless
u, v	dimensionless velocity components in x and y direction
U, V	dimensional velocity components
x, y	dimensionless Cartesian coordinates

Greek symbols

α	thermal diffusivity (m^2/s)
β	coefficient of thermal expansion (K^{-1})
ν	kinematic viscosity (m^2/s)

Subscripts

av	average
c	cold wall
l	local
max	maximum

Superscript

$*$	dimensional form

is varied up to 12,000, Gr is varied between 10^7 to 5×10^9 such a way that the Richardson number Gr/Re^2 is within 0.1 to 1000. The correlation of Nu has been presented as a function of Re, Gr/Re^2 and depthwise aspect ratio. They have concluded that it remains insensitive of the Richardson number.

Second type of problem deals with a side driven differentially heated cavities. Here, the left vertical wall is moving with constant velocity and all the other three walls remain stationary. Two different orientations of thermal boundary conditions at the vertical walls are considered in order to simulate buoyancy-aiding and buoyancy-opposing flows. Aydin [5] has considered the top and the bottom walls as adiabatic. The computations are done for $Re = 100$, $Pr = 0.71$ and Gr/Re^2 range from 0.01 to 100. It was found that the mixed-convection range of Gr/Re^2 for the opposing-buoyancy case was seen to be wider than the aiding-buoyancy case. Oztop and Dagtekin [6] have considered that the vertical walls have different constant temperatures and the horizontal walls are adiabatic. Three case are considered, viz. (a) the left wall (cold) is moving up while right wall (hot) is moving down, (b) the left wall is moving down and the right wall is moving upwards, (c) both the vertical walls are moving upwards. Governing parameters are $0.01 < Gr/Re^2 < 100$ and $Pr = 0.7$. It is found that both Ri and the direction of moving walls affect the fluid flow and heat transfer. For $Ri < 1$, the influence of the moving walls on the heat transfer is the same when they move in the opposite direction regardless of which side moves upwards and it is reduced when both move upwards. For $Ri > 1$, there is a marginal increase in heat transfer in case of opposing buoyancy and shear force due to the particular flow structure.

The bifurcation study has been conducted by Goodrich et al. [7]. It has been shown that with the increase in Re, the total kinetic energy (TKE) does not remain steady. It shows an oscillation which means that the flow no more remains a steady. It undergoes a bifurcation and finally becomes an unsteady one. A bifurcation study of buoyant horizontal laminar jet has been conducted by Arakeri et al. [8]. They have shown that under certain conditions, the jet has been found to undergo bifurcation. The bifurcation of the jet occurs in a limited domain of Grashof number and Reynolds Number. They have mapped the region in Re–Gr plane.

The problem of mixed convection in a lid-driven cavity problem has not been studied in details earlier. In the present case, we have considered a rectangular cavity where Re has been kept at 100 while the Gr has been varied between 0, $\pm 10^4$, $\pm 10^6$ keeping the $Pr = 1$. The aspect ratio (height/width) considered is in the range of $\frac{1}{2}$, 1 and 2. An unsteady Navier–Stokes equation has been solved and the TKE is calculated for each cases. The case of Hopf bifurcation has been studied and reported here.

2. Problem specification

Fig. 1 shows the geometry of the two-dimensional lid-driven rectangular cavity filled with viscous fluid along with the boundary conditions. The two vertical walls are maintained at cold temperature $T = 0$ where as in one case the top-moving wall is maintained at hot $T = 1$ and the bottom is cold $T = 0$ and in the other case, the top is cold $T = 0$ and the bottom is hot $T = 1$. Depending upon these two situations, the Grashof number will be either positive or negative (discussed later). In all the cases, the gravity

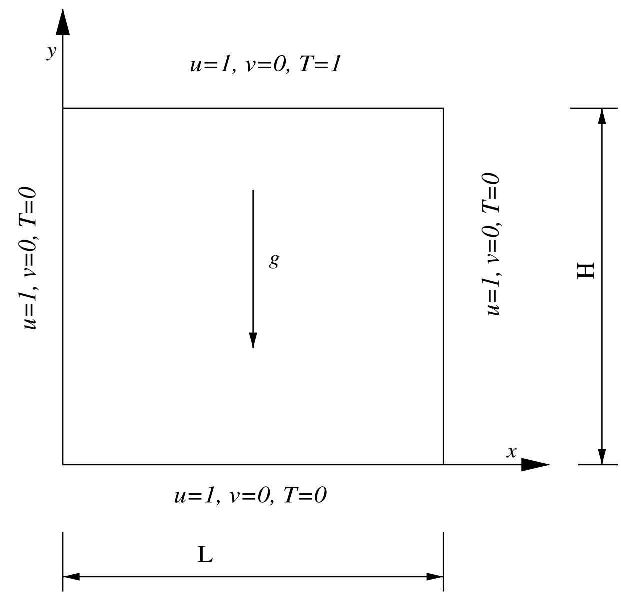

Fig. 1. Boundary conditions.

vector is acting in the negative y-direction (parallel to the vertical walls). The aspect ratio is defined as the ratio of height to width i.e. H/L. Three values are considered viz. $\frac{1}{2}$, 1 and 2.

3. Governing equations

Natural convection is governed by the differential equations expressing the conservation of mass, momentum, and energy. The present flow is considered steady, laminar, incompressible and two-dimensional. The viscous dissipation term in the energy equation is neglected. The variation of fluid properties with temperature has been neglected, with the only exception of the buoyancy term, for which the Boussinesq approximation has been adopted.

The governing equations and the boundary conditions can be transformed to dimensionless form by using appropriate normalization. Velocities can be normalized by a reference velocities U, spatial coordinates by a reference length L, time by some reference time t_r, pressure by ρU^2, temperature by some reference temperature difference ΔT^*

$$x = \frac{x^*}{L}; \quad y = \frac{y^*}{L}; \quad u = \frac{u^*}{U}; \quad v = \frac{v^*}{U}; \quad p = \frac{p^*}{\rho U^2};$$
$$T = \frac{T^* - T_c}{\Delta T^*}; \quad t = \frac{t^* U}{L} \tag{1}$$

After the nondimensionalization, the governing equations will be in the following form:

Continuity equation:

$$\frac{\partial u}{\partial x} + \frac{\partial v}{\partial y} = 0 \tag{2}$$

x-momentum equation:

$$\frac{\partial u}{\partial t} + \frac{\partial (u^2)}{\partial x} + \frac{\partial (uv)}{\partial y} = -\frac{\partial p}{\partial x} + \frac{1}{Re}\left(\frac{\partial^2 u}{\partial x^2} + \frac{\partial^2 u}{\partial y^2}\right) \tag{3}$$

y-momentum equation:

$$\frac{\partial v}{\partial t} + \frac{\partial (uv)}{\partial x} + \frac{\partial (v^2)}{\partial y} = -\frac{\partial p}{\partial y} + \frac{1}{Re}\left(\frac{\partial^2 v}{\partial x^2} + \frac{\partial^2 v}{\partial y^2}\right) + \frac{Gr}{Re^2} T \tag{4}$$

Energy equation:

$$\frac{\partial T}{\partial t} + \frac{\partial (uT)}{\partial x} + \frac{\partial (vT)}{\partial y} = \frac{1}{RePr}\left(\frac{\partial^2 T}{\partial x^2} + \frac{\partial^2 T}{\partial y^2}\right) \tag{5}$$

Table 1(a)
Comparison for Rayleigh number $Ra = 10^3$

$Ra = 10^3$	a	b	c	d	error $= \frac{a-d}{a} \times 100$
Ψ_{mid}	1.174	–	–	1.175	−0.0852
u_{max}	3.649	3.544	3.544	3.647	0.0548
at y	0.813	0.832	0.814	0.815	
v_{max}	3.697	3.593	3.586	3.707	−0.2705
at x	0.178	0.168	0.186	0.178	
Nu_{max}	1.505	1.496	1.540	1.5093	−0.2857
at y	0.092	0.0825	0.142	0.093	
Nu_{min}	0.692	0.720	0.727	0.6899	0.303
at y	1.0	0.9925	0.991	0.991	
$\overline{Nu}$	1.118	1.108	1.141	1.0998	1.6279

Table 1(b)
Comparison for Rayleigh number $Ra = 10^4$

$Ra = 10^4$	a	b	c	d	error $= \frac{a-d}{a} \times 100$
Ψ_{mid}	5.0754	–	–	5.075	0.0079
u_{max}	16.178	16.18	15.995	16.1415	0.2256
at y	0.823	0.832	0.814	0.822	
v_{max}	19.617	19.44	18.894	19.66	−0.2192
at x	0.119	0.113	0.103	0.111	
Nu_{max}	3.528	3.482	3.84	3.5584	−0.8617
at y	0.143	0.1425	0.141	0.144	
Nu_{min}	0.586	0.643	0.670	0.581	0.8532
at y	1.0	0.9925	0.991	0.9915	
$\overline{Nu}$	2.243	2.201	2.29	2.217	1.1591

Table 1(c)
Comparison for Rayleigh number $Ra = 10^5$

$Ra = 10^5$	a	b	c	d	error $= \frac{a-d}{a} \times 100$
Ψ_{mid}	9.111	–	–	9.1335	−0.2469
u_{max}	34.73	35.73	37.144	34.293	1.2583
at y	0.855	0.857	0.855	0.856	
v_{max}	68.59	69.08	68.91	68.751	−0.2347
at x	0.066	0.067	0.061	0.0593	
Nu_{max}	7.117	7.626	8.93	7.9367	−11.5175
at y	0.081	0.0825	0.080	0.0762	
Nu_{min}	0.729	0.824	1.01	0.71728	1.6076
at y	1.0	0.9925	1.0	0.9915	
$\overline{Nu}$	4.519	4.430	4.964	4.4979	0.467

where

$$Gr = \frac{g\beta\Delta TL^3}{\nu^2}; \quad Pr = \frac{\nu}{\alpha}; \quad Re = \frac{UL}{\nu} \tag{6}$$

In addition, the velocity and temperature boundary conditions, take the following form:

Table 1(d)
Comparison for Rayleigh number $Ra = 10^6$

$Ra = 10^6$	a	b	c	d	error $= \frac{a-d}{a} \times 100$
Ψ_{mid}	16.32	–	–	16.7152	−2.4215
u_{max}	64.63	68.81	66.42	65.572	−1.4575
at y	0.850	0.870	0.897	0.83898	
v_{max}	217.36	221.8	226.4	219.668	−1.0618
at x	0.0379	0.0375	0.0206	0.04237	
Nu_{max}	17.925	17.872	21.41	19.269	−7.4979
at y	0.0378	0.0375	0.030	0.0254	
Nu_{min}	0.989	1.232	1.58	0.9418	4.7725
at y	1.0	0.9925	1.0	0.9915	
$\overline{Nu}$	8.799	8.754	10.39	8.918	−1.3524

(a) Solution of [13], (b) solution of [14]; (c) solution of [15] and (d) present solution.

$$\text{Two vertical walls}: \quad u = v = T = 0$$

$$\text{for } x = 0, 1 \text{ and } 0 \leqslant y \leqslant \frac{H}{L} \tag{7}$$

$$\text{Bottom wall}: \quad u = v = T = 0$$

$$\text{for } y = 0 \text{ and } 0 \leqslant x \leqslant 1 \tag{8}$$

$$\text{Top wall}: \quad u = 1, \quad v = 0 \quad \text{and} \quad T = 1$$

$$\text{for } y = \frac{H}{L} \text{ and } 0 \leqslant x \leqslant 1 \tag{9}$$

In another case, the bottom wall is maintained at $T = 1$ and the top wall is maintained at $T = 0$.

The analysis was done for positive and negative Grashof numbers. The algebraic sign of Grashof number is determined by the definition of Grashof number given in Eq. (6). Gravity is directed downward and all terms are positive except the temperature difference (ΔT). The case $Gr > 0$ corresponds to a hot upper wall and the case $Gr < 0$ to a cold upper wall. For all calculations Reynolds number is 100.0 and Prandtl number is 1.0. The computation has been carried out for three aspect ratios viz. 1/2, 1, 2. The aspect ratio is defined as the ratio of height of the cavity to the length of the cavity. $Gr = 0$ corresponds to a lid-driven cavity flow problem.

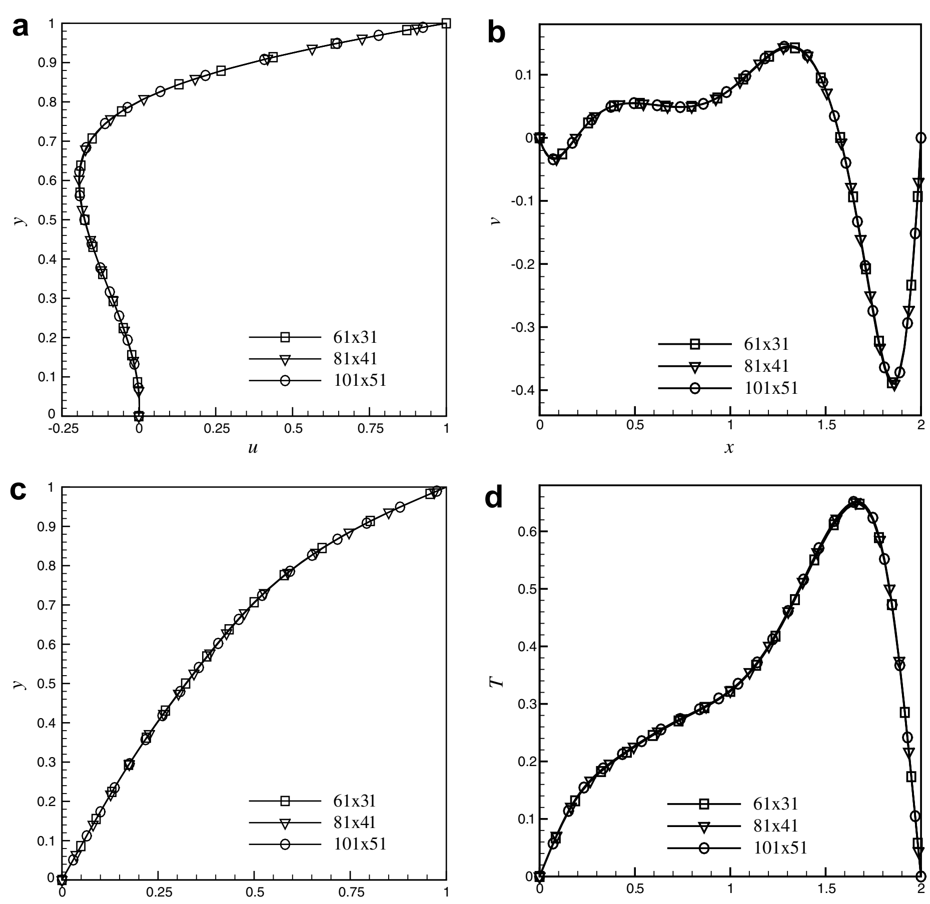

Fig. 2. Grid independence study for $Gr = 10^4$: (a) velocity at vertical mid-plane, (b) velocity at horizontal mid-plane, (c) temperature at vertical mid-plane and (d) temperature at horizontal mid-plane.

4. Numerical procedure

The SIMPLE algorithm [9] is used to couple the momentum and the continuity equations. The deferred QUICK scheme of Hayase et al. [10] is employed to minimize the numerical diffusion for the convective terms for both the momentum equations and the energy equation. The solution of the discretized momentum and pressure correction equation is obtained by line-by-line method [9]. The fully implicit scheme of Patankar [9] is followed for the numerical solution of the transient equation. Under-relaxation factor for pressure with values of 0.01 was used.

The iterative procedure is initiated by the solution of energy equation followed by momentum equations and is continued until steady-state is arrived at. At every time

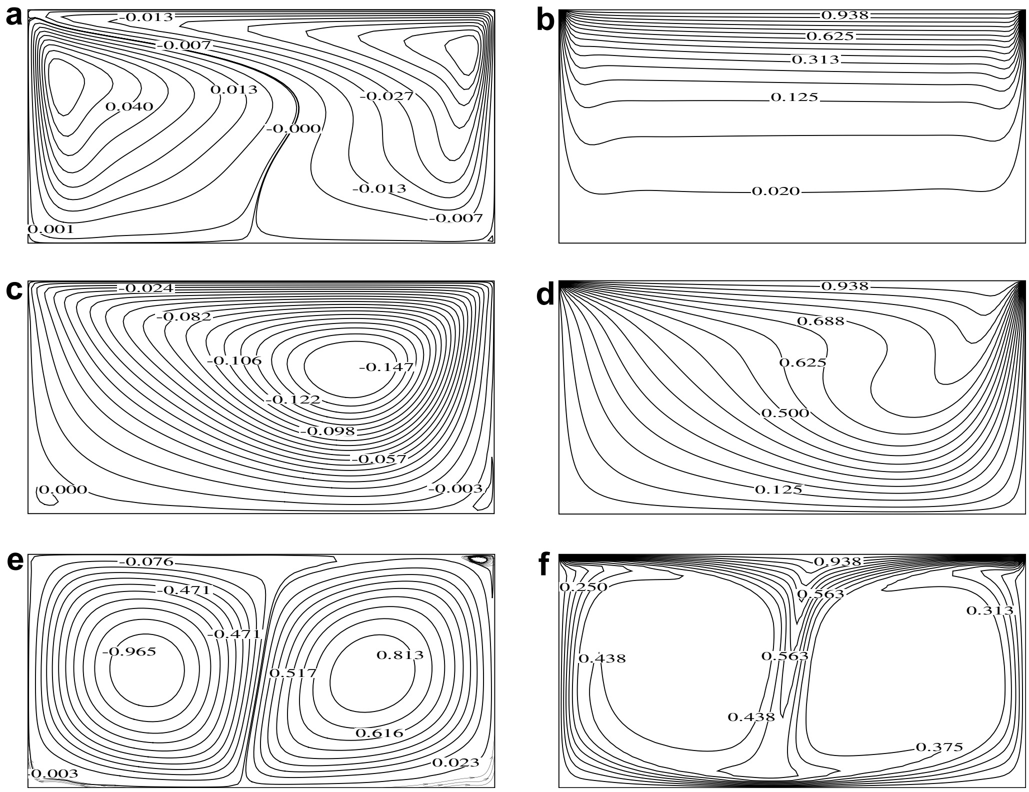

Fig. 3. Streamlines and isotherms for $Gr = 10^6$, 0 and -10^6: (a) streamlines ($Gr = 10^6$), (b) isotherms ($Gr = 10^6$), (c) streamlines ($Gr = 0$), (d) isotherms ($Gr = 0$), (e) streamlines ($Gr = -10^6$) and (f) isotherms ($Gr = -10^6$).

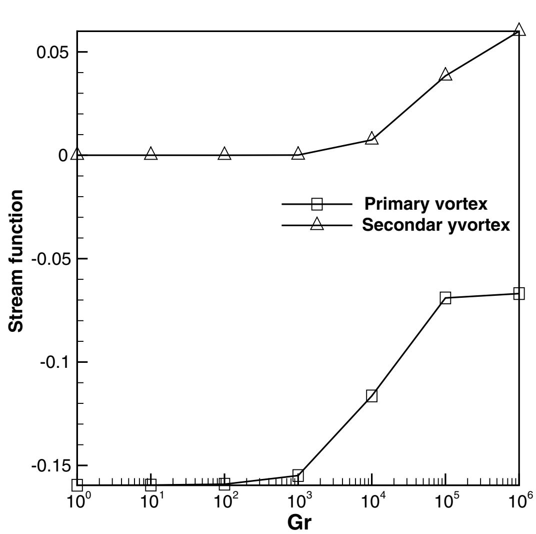

Fig. 4. Stream function at various positive Grashof numbers: AR = 0.5.

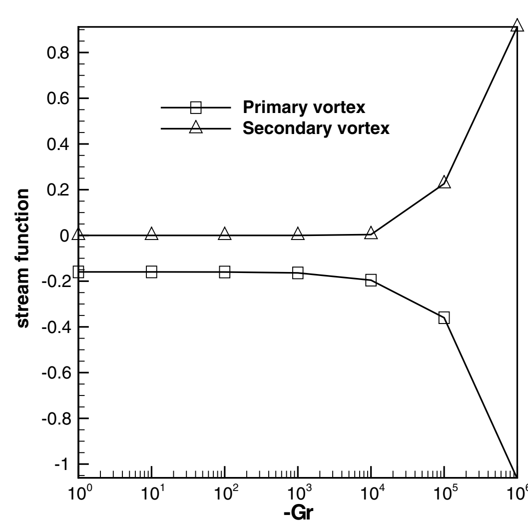

Fig. 5. Stream function at various negative Grashof numbers: AR = 0.5.

step, the global convergence is satisfied [9]. Euclidean norm of the residual is taken as convergence criteria for each dependent variable in the entire flow field [11]. The mass balance for global convergence was taken as 10^{-8}.

5. Validation of the code

Simple geometry, unambiguous flow boundary conditions and recirculating flow with multiple vortex formation have justified the use of the problem of lid driven cavity without thermal effects as a bench-mark solution for validation of CFD algorithm against other than benchmark computation [12]. On the other hand, the free convection of a viscous fluid in a differentially heated cavity with two opposing walls held at different temperatures provides another simple problem, studied extensively [13] to understand the interaction between buoyancy and shearing forces in such flow situation.

The results obtained from the present computation have been compared with the results of de Vahl Davis [13], Markatos and Perikleous [14] and Hadjisophocleous et al. [15] and presented in Tables 1(a), 1(b), 1(c), 1(d). These results are presented after conducting the grid independence test and test for different time steps. A grid size of 61 × 61 and time step size of 0.01 is considered for these computations. It is observed that the present computations are matching very close to those of Vahl Davis [13]. Similar study has been conducted for lid-driven cavity flow problem of Ghia et al. [12] for Re up to 7500. A very good matching has been obtained up to this number. Since in the present case, the Re considered in 100, these results are not presented. The detailed validation is given in Prasad [16].

6. Grid independence study

The present problem has been solved for three aspect ratios. A detailed grid independence and time independence study has been carried out for these three cases.

- Aspect ratio $\frac{1}{2}$.
  The grid independence study is shown in Fig. 2. The velocity and the temperature plots are shown. It is seen that the grid size of 81 × 41 is sufficient. However we have used 101 × 51 grids for computation. It is seen that $dt = 0.001$ is sufficient for this case.

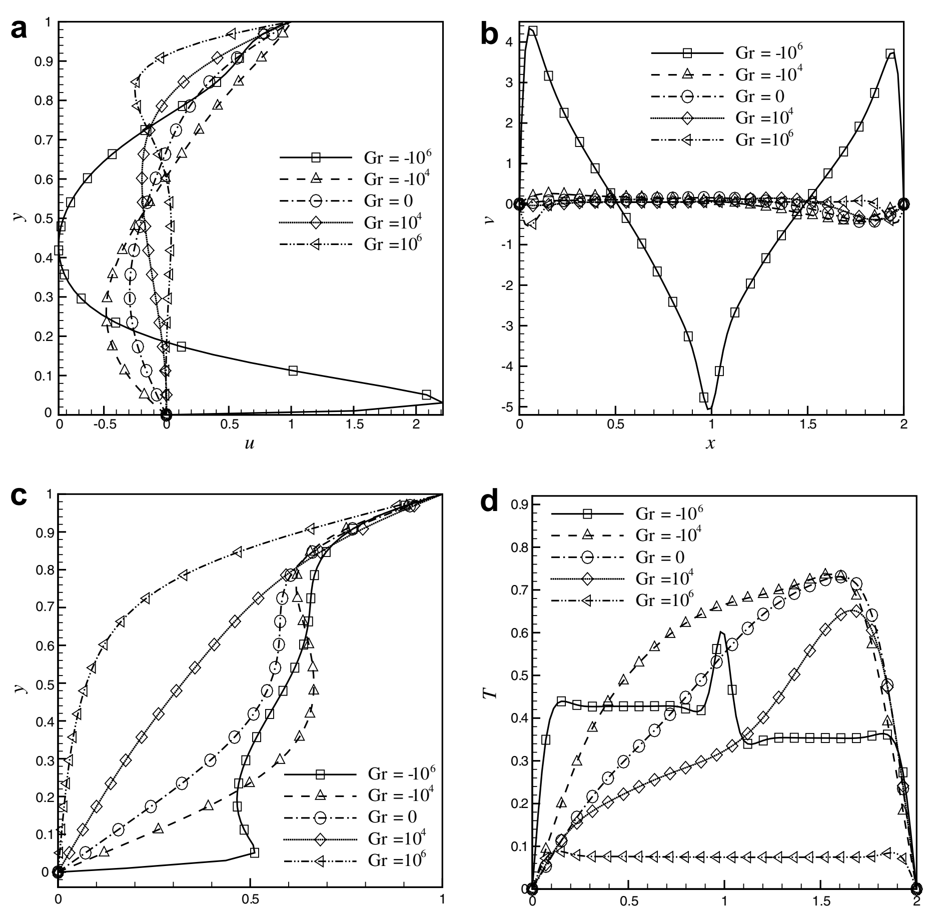

Fig. 6. Velocity and temperature profiles for various Grashof numbers: (a) velocity at vertical mid-plane, (b) velocity at horizontal mid-plane, (c) temperature at vertical mid-plane and (d) temperature at horizontal mid-plane.

- Aspect ratio 1.0.
  The grid independence study has been carried out for this aspect ratio. It is seen that the grid size of 81×81 is sufficient. The time step independence study shows that $\mathrm{d}t = 0.01$ is sufficient for this case. However, we have used $\mathrm{d}t = 0.001$ for computation.
- Aspect ratio 2.0.
  The grid independence study has been carried out for this aspect ratio. It is seen that the grid size of 41×81 is sufficient. However, we have used 51×101 for further computation. The time step independence study shows that $\mathrm{d}t = 0.001$ is sufficient for this case.

7. Results and discussion

Results are presented for mixed convection inside a rectangular cavity where the Gr has been varied between 0, $\pm 10^4$, $\pm 10^6$ keeping Re at 100 and $Pr = 1$. The aspect ratio (height/width) considered is in the range of $\frac{1}{2}$, 1 and 2.

7.1. Aspect ratio, AR = 0.5

The aspect ratio is the ratio of the height (H) and width (i.e., length L). The aspect ratio with AR = 0.5 is a rectangular geometry of height 1.0 and width 2.0.

Streamlines and isotherms for the range of Grashof numbers ($-10^6 \leqslant Gr \leqslant 10^6$) are shown in the Fig. 3. Negative and positive values of the stream function correspond to clockwise and counter-clockwise circulation respectively. The relative maximum value of stream function corresponds to the center of the vortex. The point of the relative minimum value of stream function corresponds to the points of detachment of the boundary layers from the wall due to flow separation.

The primary vortex is generated by the motion of moving wall. The secondary vortex is formed near the corners due to the separation of the boundary layer growing along the bottom horizontal wall, under the adverse pressure gradient caused by the stagnation effect of the perpendicular wall.

The streamline and isotherm plots for $Gr = 10^6$, 0 and -10^6 are shown in Fig. 3. The Richardson number ($Ri = Gr/Re^2$) are 100, 0 and -100, respectively (because $Re = 100$). The right vortex (primary vortex) is originated due to the movement of the wall and the left side vortex (secondary vortex) is due to the natural convection. It is to be noted that on the right wall, the buoyancy and shear forces are in aiding combination whereas on the left wall they are opposing each other. With the decrease of Ri, it is observed that the relative size of the primary vortex is

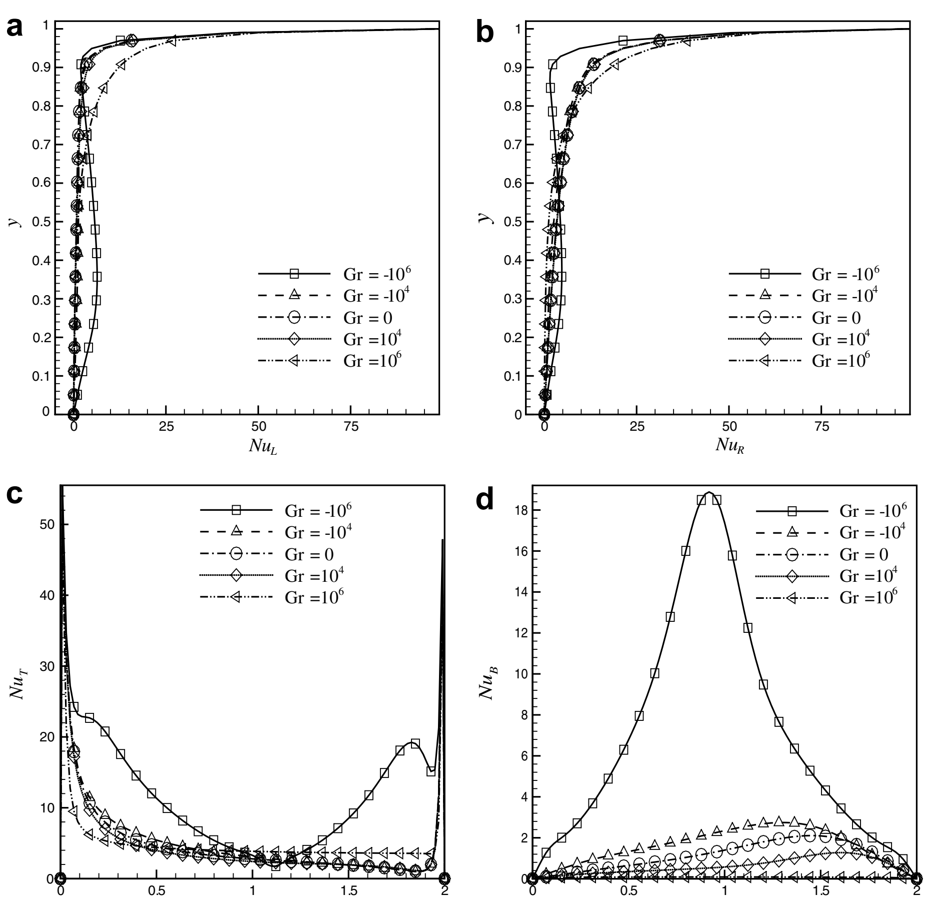

Fig. 7. Variations in the local Nu for different Grashof numbers: (a) local Nu on the left wall, (b) local Nu on the right wall, (c) local Nu on the top wall and (d) local Nu on the bottom wall.

increasing compared to the secondary vortex. For $Gr = 0$, it resembles the case of lid-driven cavity flow problem. The convection current in the isotherms are becoming predominant with the decrease of Gr.

For $Gr \geqslant 10^4$, the effect of a heated upper wall is to enhance the left corner eddy. Warm buoyant fluid tends to remain near the top. With the increase in Gr, the buoyancy force is increased which opposes the wall shear force. The net effect is that the stream function values of primary cell is decreased and the secondary cell is increased. For $Gr < 0$, the cooled upper wall has the reverse effect. The primary circulation due to the wall shear and the secondary circulation due to the buoyancy increase with the increase of Gr. As is seen from the Fig. 3c a relatively similar size of vortices are formed.

From Fig. 4, at $Gr = 10^6$ the difference of the stream function values of the primary and secondary cells are relatively less. At large Gr, the buoyancy effect is more and it opposes the convection due to the moving wall. The strength of the vortices for $-Gr$ are given in Fig. 5. The strength is far more intensive compared to the positive Gr case.

The midplane velocity and temperature distributions are shown in Fig. 6. It is seen that for $Gr = 0$, the midplane u, v and T distributions resemble that of lid-driven cavity flow problem. As Gr is increased to 10^6, the convection effects are not much predominant (Fig. 6a and b) and that is the reason why a boundary layer type of profile is seen in Fig. 6c and the core is largely uniform small temperature (Fig. 6d). However, the convection strength is very high which is observed in the Fig. 6a and b. In the vertical mid-plane, there is a steep gradient at $y = 0$ (Fig. 6c) and in the middle of the core, there is a large temperature variation (Fig. 6d).

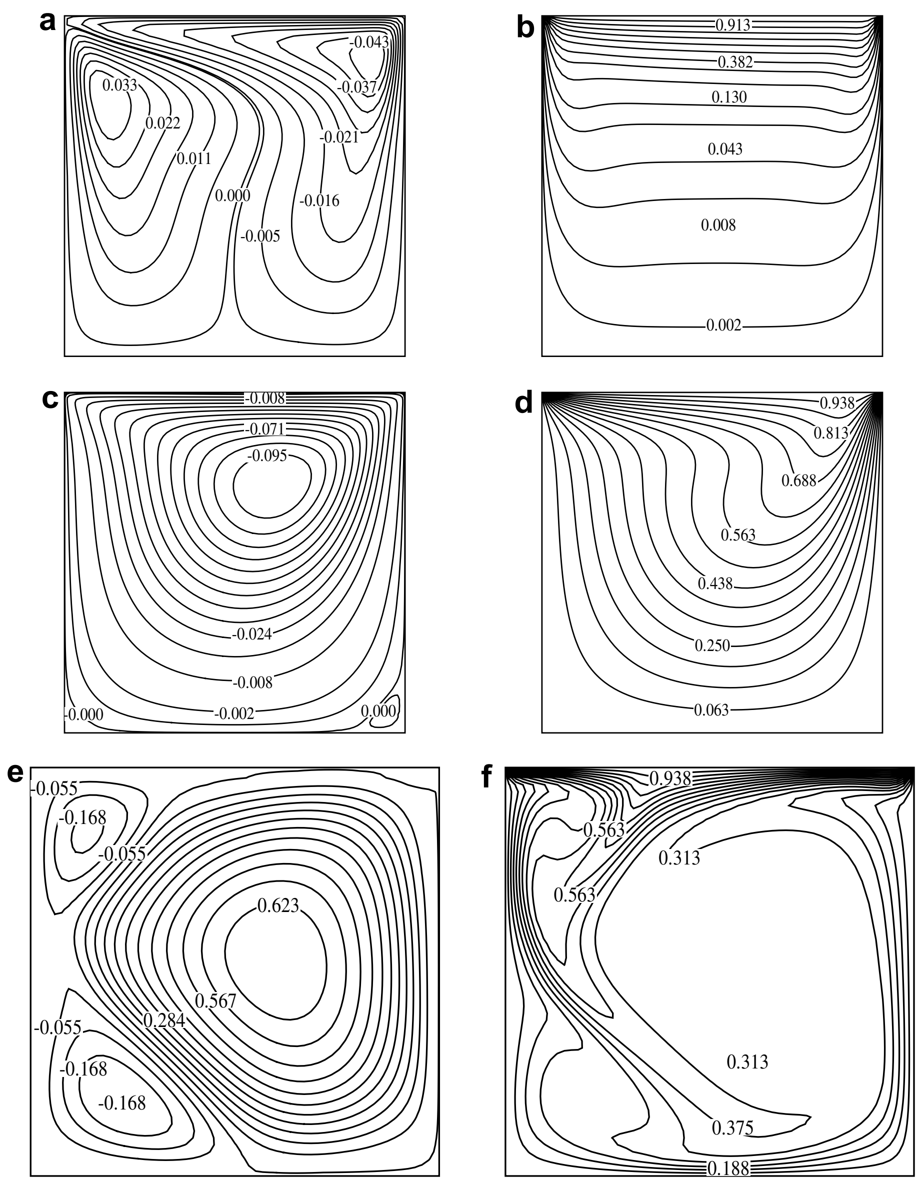

Fig. 8. Streamlines and isotherms for $Gr = 10^6, 0, -10^6$: (a) streamlines ($Gr = 10^6$), (b) isotherms ($Gr = 10^6$), (c) streamlines ($Gr = 0$), (d) isotherms ($Gr = 0$), (e) streamlines ($Gr = -10^6$) and (f) isotherms ($Gr = -10^6$).

The convection pattern as discussed is reflected on the *Nu* distribution on the four walls (Fig. 7). On the two vertical walls, the *Nu* distribution is not affected by the positive or negative *Gr* (Fig. 7a and b). However, on the bottom and top walls, *Nu* remains largely unaffected by the variation of positive *Gr* whereas for negative *Gr*, there is a large variation of *Nu* because of the flow adjustments in this range (Fig. 7c and d).

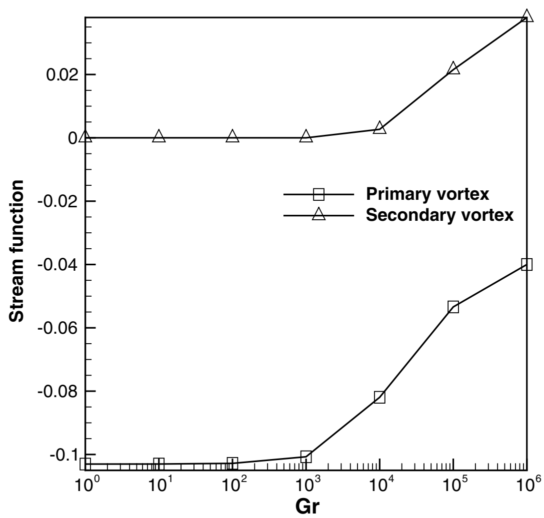

Fig. 9. Stream function at various positive Grashof numbers: AR = 1.

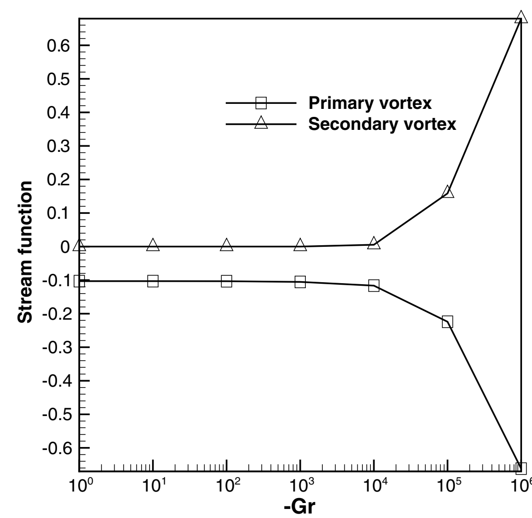

Fig. 10. Stream function at various negative Grashof numbers: AR = 1.

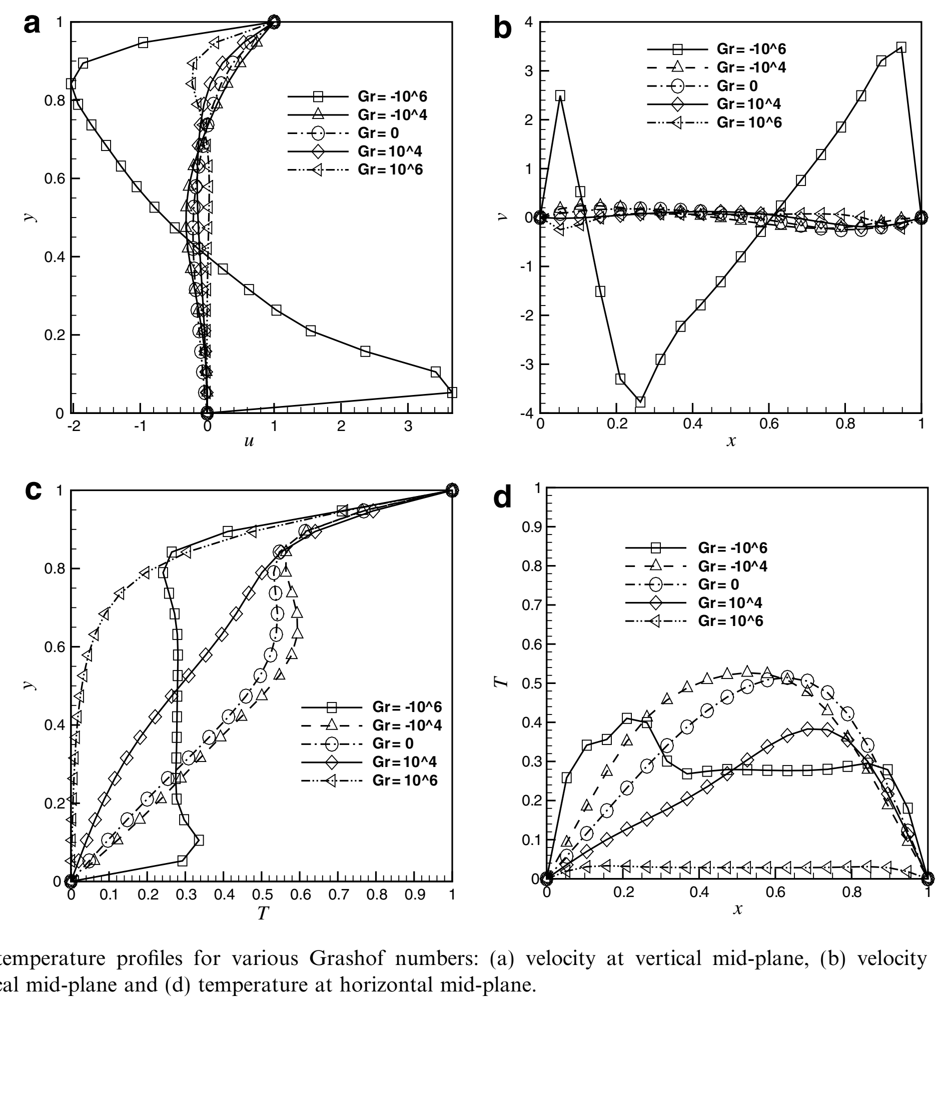

Fig. 11. Velocity and temperature profiles for various Grashof numbers: (a) velocity at vertical mid-plane, (b) velocity at horizontal mid-plane, (c) temperature at vertical mid-plane and (d) temperature at horizontal mid-plane.

7.2. Aspect ratio, AR = 1.0

The aspect ratio with AR = 1.0 is a square geometry of same height and width. The streamlines and isotherms in the range of $-10^6 \leqslant Gr \leqslant 10^6$ are shown in Fig. 8. When $Gr = 10^6$ (Fig. 8a), it is observed that the primary cell due to the lid-movement and the secondary cell due to the buoyancy are relatively similar in size. However, since the buoyancy is high ($Ri = 100$), the temperature contour has the pattern of a thermally stratified nature and convection is almost absent. With the decrease of *Gr*, the secondary cell is gradually diminishing and finally at $Gr = 0$, it has disappeared. The point to note is that gradually the convection effect in heat transfer is increasing (as seen in the isotherm contours) because of the same reason. For $Gr = 10^4$ (not shown), the separation takes place on the bottom wall at $x = 0.4$ and fluid strikes the left wall at $y = 0.65$. With the increase in *Gr*, the secondary cell becomes stronger due to the buoyancy force which weakens the primary cell. For $Gr = 10^5$ (not shown), the primary cell strikes the left wall at $y = 0.85$ and for $Gr = 10^6$, at $y = 0.98$ due to increased buoyancy force. As the negative *Gr* is gradually increased up to 10^2 (not shown), it is observed that the flow is largely dominated by the lid-movement i.e. convection due to the buoyancy is absent. Similar type of nature has also been reported by Dalal and Das [17]. As the $-Gr$ is increased to 10^4 (not shown), the secondary cell has appeared which increases in size and finally at $-Gr = 10^6$, the primary cell is broken into two smaller cell. It is observed that the heat convection has increased to a higher level.

As in the case of AR = 0.5, the difference between the two stream-function values are relatively less at $Gr = 10^6$ compared to $Gr = 10^0$ (Fig. 9). With the increase in negative *Gr*, the strength of convection increases (Fig. 10).

The velocity and temperature distribution along vertical and horizontal mid-planes are shown in Fig. 11. For different Grashof numbers, it is observed that they have similar trends. The velocity and temperature distributions are shown along vertical mid-plane (Fig. 11a and c) and horizontal mid-plane (Fig. 11b and d). Both u and v velocities are affected by a large amount for $Gr = -10^6$. For other *Gr*, the variations is less. The same is reflected in the temperature distribution. As the *Gr* is reduced from 10^6 to 0, a thermally stratified field gives way to a forced convection dominated flow. With increase in negative *Gr*, however, the natural convection dominates and thus the core largely remains isothermal (Fig. 11c) whereas the temperature var-

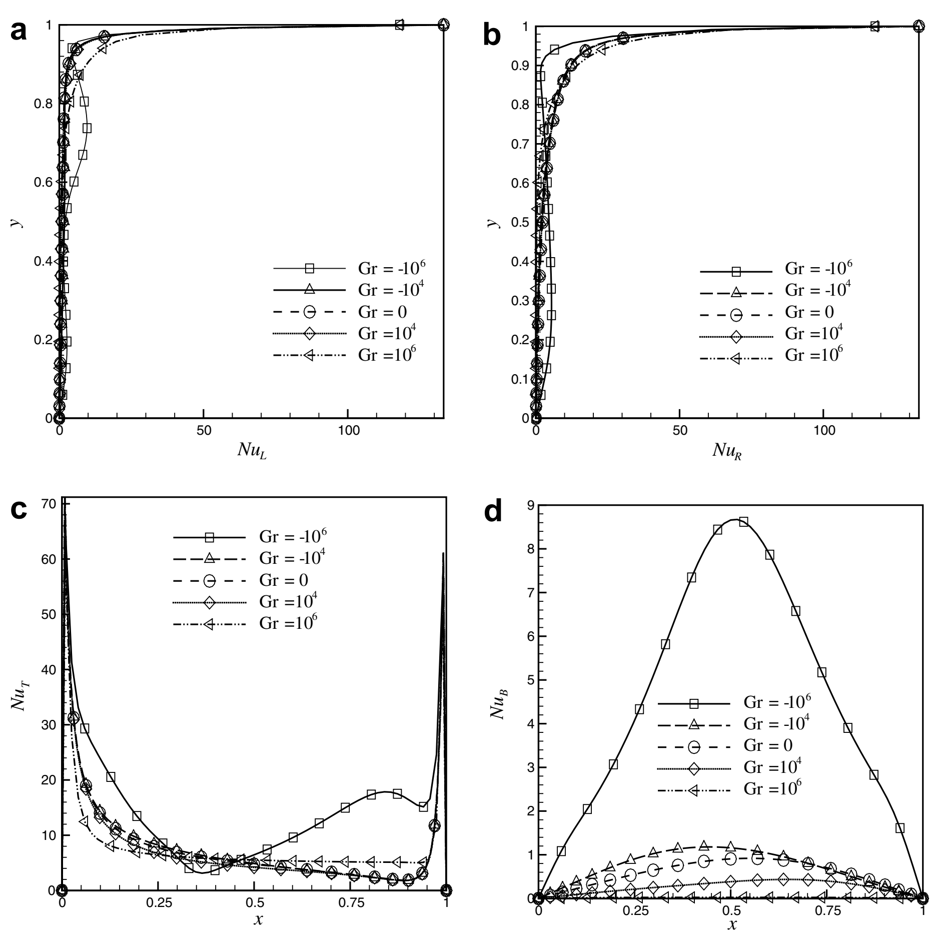

Fig. 12. Variations in the local *Nu* for different Grashof numbers: (a) local *Nu* on the left wall, (b) local *Nu* on the right wall, (c) local *Nu* on the top wall and (d) local *Nu* on the bottom wall.

iation is more near the boundaries. The isothermal core is also seen to be present partly in Fig. 11d.

The Nu distribution on the four walls are shown in Fig. 12a–d. The Nusselt number is maximum at the top

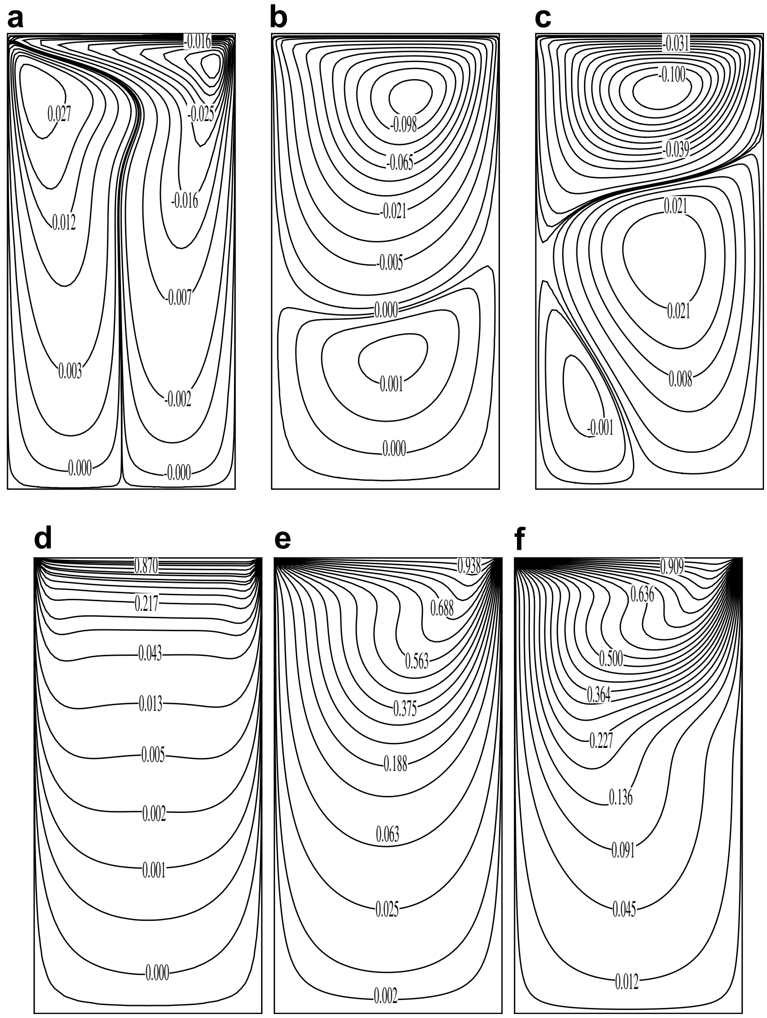

Fig. 13. Streamlines and isotherms for $Gr = 10^6, 0, -10^4$: (a) streamlines ($Gr = 10^6$), (b) streamlines ($Gr = 0$), (c) streamlines ($Gr = -10^4$), (d) isotherms ($Gr = 10^6$), (e) isotherms ($Gr = 0$) and (f) isotherms ($Gr = -10^4$).

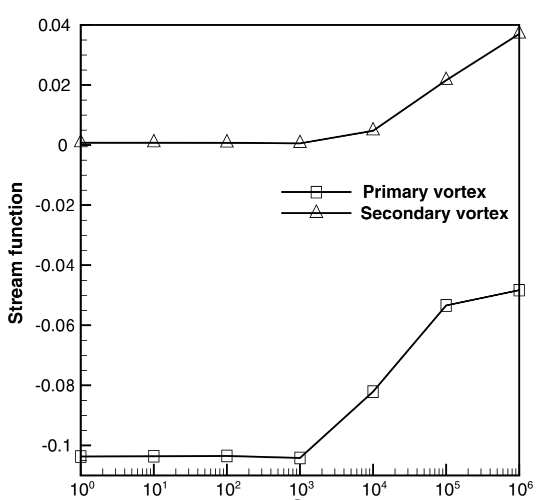

Fig. 14. Stream function at various positive Grashof numbers: AR = 2.

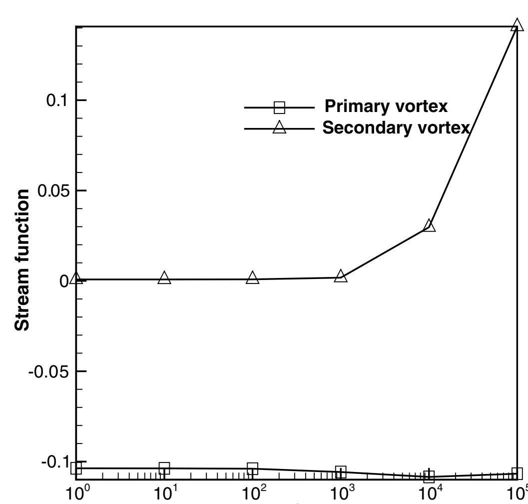

Fig. 15. Stream function at various negative Grashof numbers: AR = 2.

wall and minimum on the left wall. There is a remarkable contribution from the bottom wall. On the bottom wall, local Nusselt number is relatively less for $Gr = 10^6$ compared to $Gr = -10^6$. This is because in the first case, the top wall is hot which gives rise to the thermally stratified situation (Fig. 8b) whereas in the second case, the bottom wall is heated which gives rise to the buoyancy effect (Fig. 8f). For negative Grashof number, average *Nu* is maximum at the top wall for all *Gr*. However, for $Gr = -10^6$, the formation of the boundary layer is to be noted on the top wall and as a consequence of it, the *Nu* distribution has a wavy pattern. The Nusselt number of the two vertical walls are not affected by the variation of *Gr* in the range of 10^6 to -10^6.

7.3. Aspect ratio, AR = 2.0

Aspect ratio with AR = 2.0 is a rectangular geometry of height 2.0 and width 1.0. The streamlines and isotherm pattern for $Gr = -10^4$, 0 and 10^4 are shown in Fig. 13. The natural convection effect is increased with the increase in *Gr* and it is seen that for $Gr = 10^6$, the bottom vortex takes the shape of a secondary vortex (Fig. 13a). For $Gr = 10^2$ (not shown), the thermal convection is seen to be present while for $Gr = 10^6$, this thermal convection is suppressed and a thermally stratified field is present. As the *Gr* is gradually decreased, the vortices one above the other are becoming visible which is a characteristics of forced convection in a rectangular cavity [18]. The streamline pattern in a rectangular cavity with AR = 2 for forced convection case ($Gr = 0$) has been studied by Cortes and Miller [18]. Two vortices are seen to be present: one on the top and another at the bottom. As $-Gr$ is increased, a complex flow phenomenon is observed beyond 10^4. At higher $-Gr = 10^5$ (not shown), the flow becomes more complex and it will be shown later that the flow does not remain steady. A Hopf bifurcation occurs and unsteady behaviour is observed.

Fig. 14 shows the variation of stream function with the increase in *Gr*. It is observed that with increase in *Gr*, the strength of the secondary vortex increases whereas the strength of the primary vortex decreases. The strength of convection as represented by stream-function for various $-Gr$ is plotted in Fig. 15. It is observed that as the $-Gr$ is increased, the strength of primary vortex remains same whereas that of the secondary vortex increases.

The vertical and horizontal mid-plane velocity and temperature distribution are shown in Fig. 16. As mentioned, the results for $Gr = -10^6$ are not steady and only a representative value at a particular time. The velocity at two

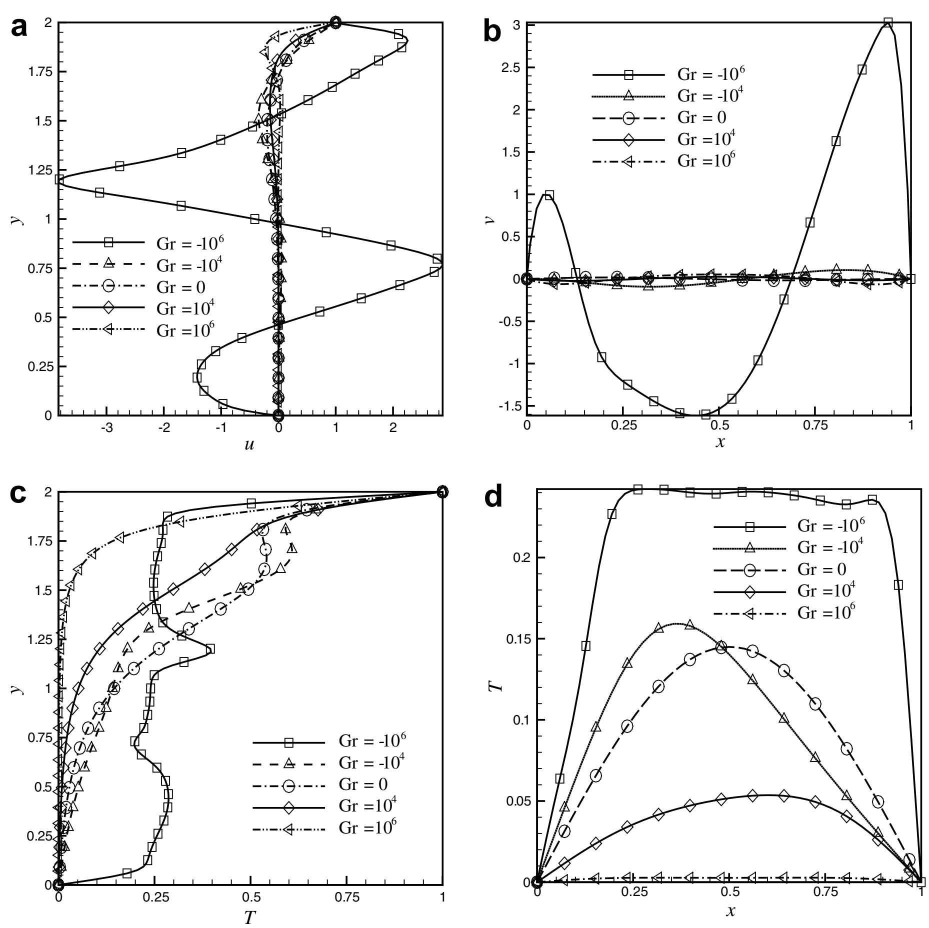

Fig. 16. Velocity and temperature profiles for different Grashof numbers: (a) velocity at vertical mid-plane, (b) velocity at horizontal mid-plane, (c) temperature at vertical mid-plane and (d) temperature at horizontal mid-plane.

mid-plane show that except $Gr = -10^6$, the changes are relatively small. The temperature distribution at two mid-plane (Fig. 16c and d) show that the conduction mode is predominant at $Gr = 10^6$ and convection mode starts dominating as $-Gr$ is increased.

The heat transfer from the four walls are represented by *Nu* distribution and shown in Fig. 17. Similar to the earlier observation for other aspect ratios, the left and right walls do not contribute to much of the heat transfer (Fig. 17a and b). The heat transfer from the top wall is shown in Fig. 17c. Except for $Gr = -10^6$, Nu_T is same order for all *Gr*. The bottom wall does not take part in heat transfer for all but except $Gr = -10^6$.

7.4. Bifurcation study

For a lid-driven cavity flow problem, it has been shown by Gustafson and Halasi [19], Goodrich et al. [7] and Goyon [20] that Hopf bifurcation occurs when *Re* is increased above certain value. The Reynolds number at which it occurs has also been established by several other authors. A similar kind of study has been conducted here to find out whether the bifurcation occurs for a combina-

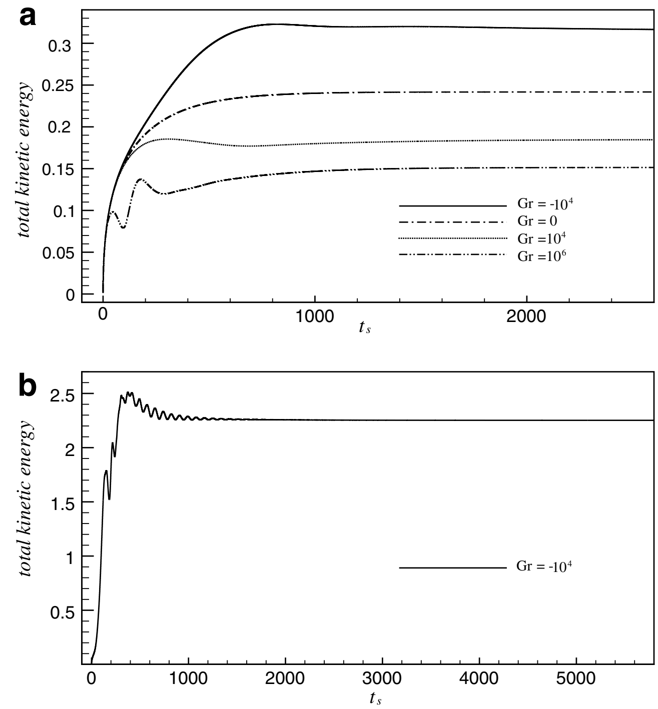

Fig. 18. Total kinetic energy for various Grashof numbers, AR = 0.5: (a) $Gr = 10^6, 10^4, 0, -10^4$ and (b) $Gr = -10^6$.

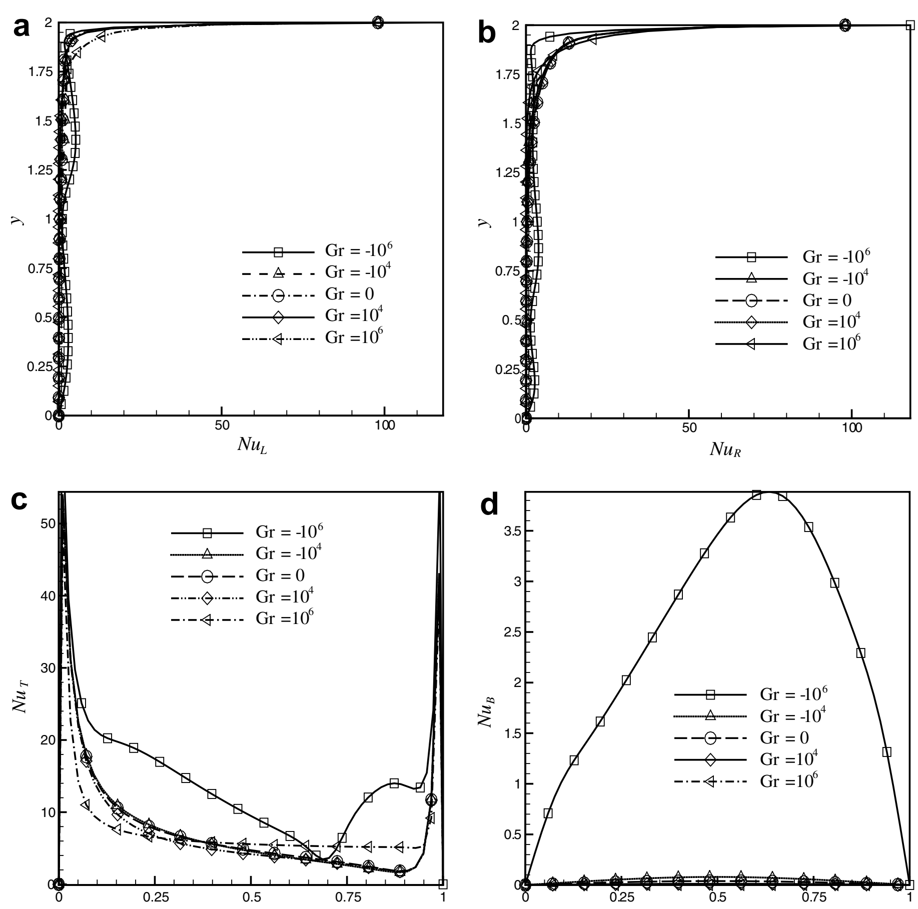

Fig. 17. Variations in the local *Nu* for different Grashof numbers: (a) local *Nu* on the left wall, (b) local *Nu* on the right wall, (c) local *Nu* on the top wall and (d) local *Nu* on the bottom wall.

tion of *Gr* and *Re*. The total kinetic energy (TKE) expression is given by Goyon [20]

$$E(n \times \mathrm{d}t) = \left(\sum_{(i,j)=(1,1)}^{(nx,ny)} [(u_{i,j}^n)^2 + (v_{i,j}^n)^2] \right)^{\frac{1}{2}} \tag{10}$$

The TKE for various *Gr* has been shown in Fig. 18 for AR = 0.5. It is observed that after initial unsteadiness, the flow becomes steady as the TKE attains a constant value. With increase in $-Gr$, the magnitude for TKE increases which is an indication of the increase of convection. The TKE for AR = 1.0 is shown in Fig. 19a–f. From Fig. 19a, it is seen that TKE is increasing as the *Gr* is varied from positive to negative value. For $Gr = -10^6$, the TKE undergoes a continuous fluctuation for a large time $t \approx 550.0$. The TKE for AR = 2.0 is shown in Figs. 20–22. The steady-state results have been obtained as the *Gr*

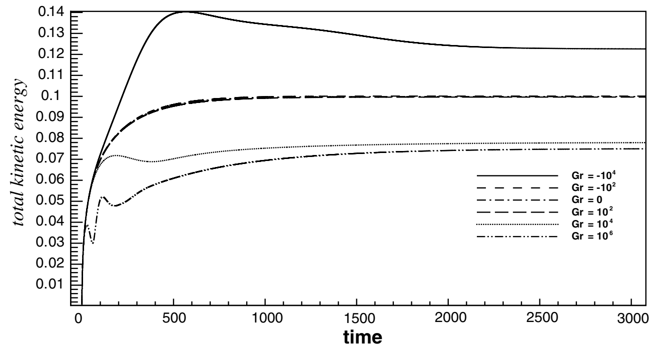

Fig. 20. Total kinetic energy for various Grashof numbers, AR = 2.0.

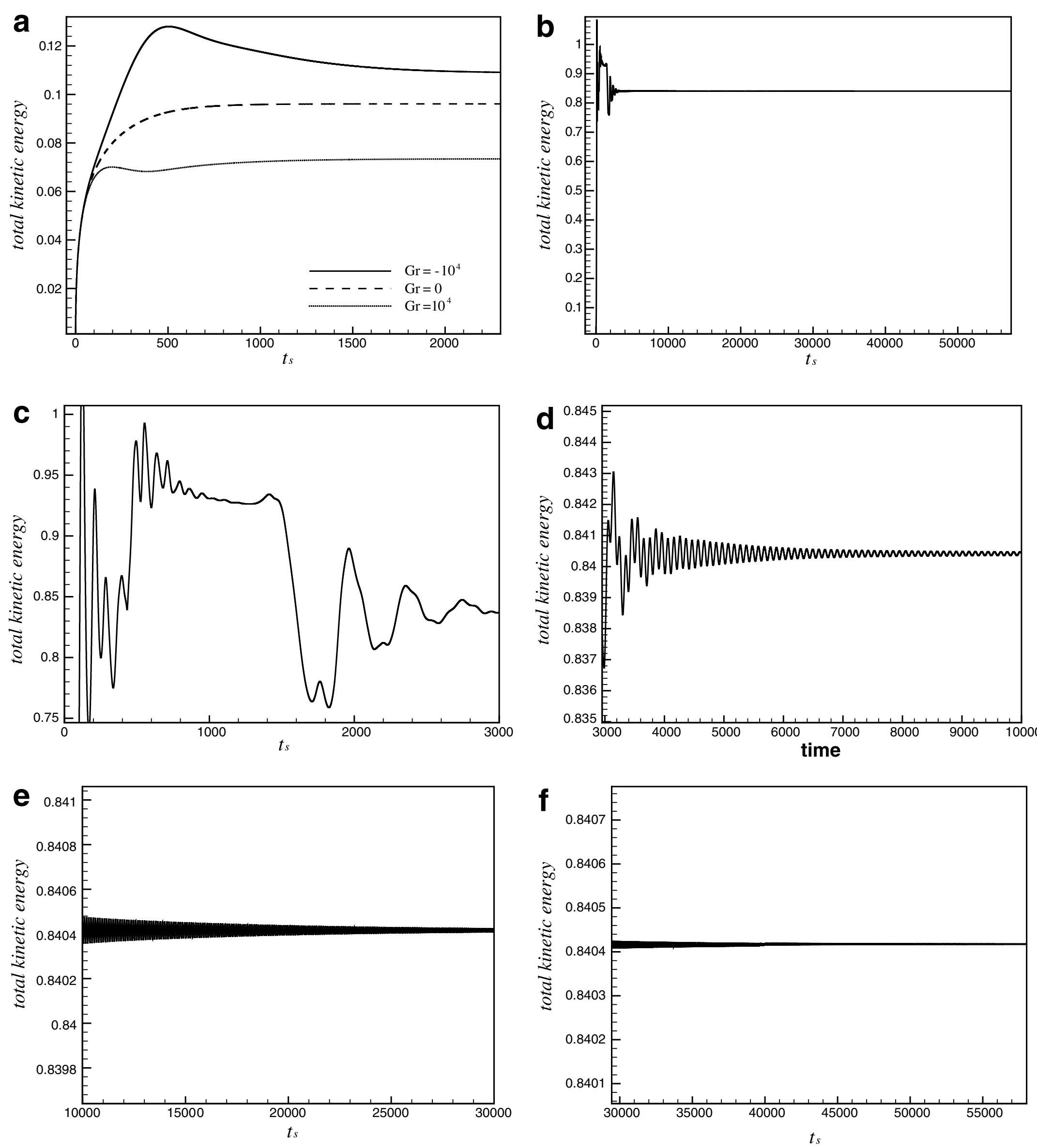

Fig. 19. Total kinetic energy (scaled time, $t_s = t \times 100$), AR = 1.0: (a) for various Grashof numbers, (b) up to $t = 600.0$ ($Gr = -10^6$), (c) up to $t = 30.0$ ($Gr = -10^6$), (d) $30.0 < t < 100.0$ ($Gr = -10^6$), (e) $100.0 < t < 300.0$ ($Gr = -10^6$) and (f) $300.0 < t < 550.0$ ($Gr = -10^6$).

is varied from 10^6 to -10^4 (Fig. 20). However, for $Gr = -10^5$, a periodic oscillation of the TKE has been observed (Fig. 21a–e). After the initial large transients, the flow exhibits a periodic oscillation (Fig. 21e). The period of oscillation computed is 4.368. It is established that the flow has undergone a Hopf bifurcation at $Gr = -10^5$ and $Re = 100$. Further, computation has been carried out for $Gr = -10^6$. The TKE distribution has been shown in Fig. 22. The magnitude of TKE has increased in this case. It is observed that the periodic oscillation is not regularly. A further study should be conducted to investigate the path leading to chaos.

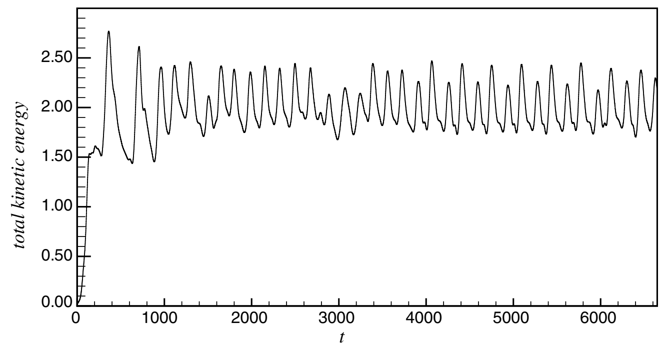

Fig. 22. Total kinetic energy for $Gr = -10^6$, AR = 2.

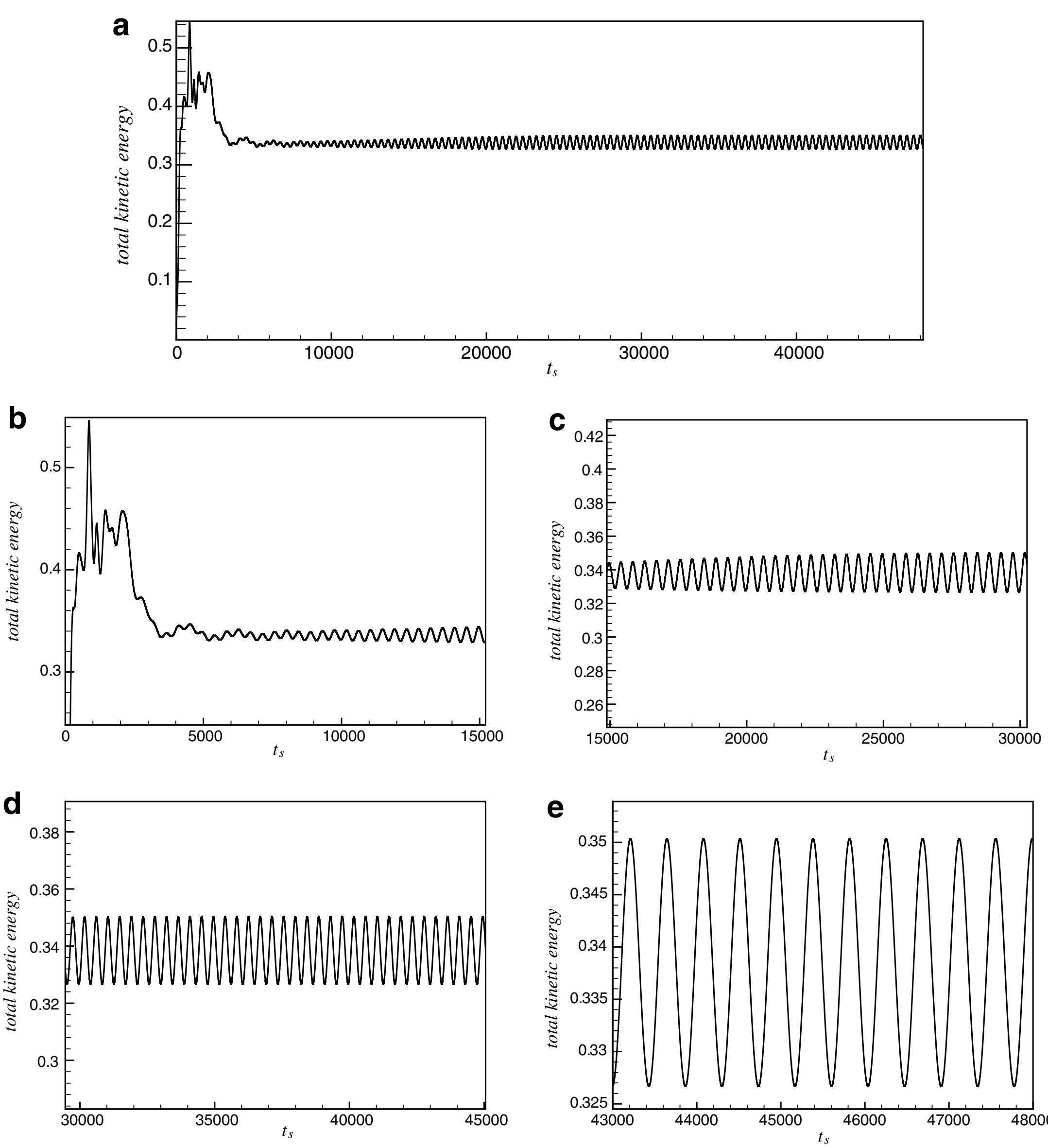

Fig. 21. Total kinetic energy for $Gr = -10^5$, AR = 2.0: (a) up to $t = 500.0$, (b) up to $t = 150.0$, (c) $150.0 < t < 300.0$, (d) $300.0 < t < 450.0$ and (e) $430.0 < t < 480.0$.

8. Conclusions

From the above study, the following conclusions may be drawn:

- As the negative *Gr* is increased, a strong convection results which is observed from the streamline and isotherm plots. For AR equal to 0.5 and 1.0, this is observed for all the *Gr*. However, for AR = 2.0, the flow undergoes a Hopf bifurcation for $-Gr = 10^5$ and above. The flow does not remain steady any longer and becomes a transient case.
- For high $-Gr$, a relatively large isothermal core is observed at the center whereas for high *Gr*, a conduction-type of temperature profile is observed.
- The left and the right walls do not have significant contribution for heat transfer. The bottom and the top walls participate mainly in heat transfer.
- For $Gr = 10^6$, temperature stratification is apparent, whereas for $Gr = -10^6$, buoyancy is effective in stimulating circulation.
- For all cavities, isotherms move towards the top for $Gr = 10^4$ and above and towards the bottom for $-Gr = 10^4$ and above as the fluid circulation is retarded or enhanced respectively.
- The TKE study shows that for AR = 0.5, and 1.0, the flow is steady for the range of *Gr* considered. For AR = 2.0, the TKE plot suggests that a periodic oscillation is obtained for $-Gr = 10^5$. This oscillation does not remain periodic when the $-Gr$ is further increased to 10^6.

References

[1] K. Torrance, R. Davis, K. Eike, P. Gill, D. Gutman, A. Hsui, S. Lyons, H. Zien, Cavity flows driven by buoyancy and shear, J. Fluid Mech. 51 (Part. 2) (1971) 221–231.
[2] R. Iwatsu, J.M. Hyun, K. Kuwahara, Mixed convection in a driven cavity with a stable vertical temperature gradient, Int. J. Heat Mass Transfer 36 (6) (1993) 1601–1608.
[3] K.M. Khanafer, A.J. Chamkha, Mixed convection flow in a lid-driven enclosure filled with a fluid-saturated porous medium, Int. J. Heat Mass Transfer 42 (13) (1999) 2465–2481.
[4] A.K. Prasad, J.R. Koseff, Combined forced and natural convection heat transfer in a deep lid-driven cavity, Int. J. Heat Fluid Flow 17 (1996) 460–467.
[5] O. Aydin, Aiding and opposing mechanisms of mixed convection in a shear- and buoyancy-driven cavity, Int. Commun. Heat Mass Transfer 26 (7) (1999) 1019–1028.
[6] H.F. Oztop, I. Dagtekin, Mixed convection in two-sided lid-driven differentially heated square cavity, Int. J. Heat Mass Transfer 47 (2004) 1761–1769.
[7] J.W. Goodrich, K. Gustafson, K. Halasi, Hopf bifurcation in driven cavity, J. Comput. Phys. 90 (1990) 219–261.
[8] J.H. Arakeri, D. Das, J. Srinivasan, Bifurcation in a buoyant horizontal laminar jet, J. Fluid Mech. 412 (2000) 61–71.
[9] S.V. Patankar, Numerical Heat Transfer and Fluid Flow, Hemisphere Publishing Co., New York, 1980.
[10] T. Hayase, J.A.C. Humphrey, R. Greif, A consistently formulated QUICK scheme for fast and stable convergence using finite-volume iterative calculation procedures, J. Comput. Phys. 98 (1) (1992) 108–118.
[11] J.P.V. Doormaal, G.D. Raithby, Enhancements of the SIMPLE method for pressure incompressible fluid flows, Numer. Heat Transfer 7 (1984) 147–163.
[12] U. Ghia, K.N. Ghia, C.T. Shin, High-*Re* solutions for incompressible flow using the Navier–Stokes equations and a multi grid method, J. Comput. Phys. 48 (1982) 387–411.
[13] G. de Vahl Davis, Natural convection of air in a square cavity: a benchmark numerical solution, Int. J. Numer. Methods Fluids 3 (1983) 249–264.
[14] N.C. Markatos, K.A. Perikleous, Laminar and turbulent natural convection in an enclosed cavity, Int. J. Heat Mass Transfer 27 (5) (1984) 755–772.
[15] G.V. Hadjisophocleous, A.C.M. Sousa, J.E.S. Venart, Prediction of transient natural convection in enclosures of arbitrary geometry using a nonorthogonal numerical model, Numer. Heat Transfer 13 (1988) 373–392.
[16] Y.S. Prasad, Transient mixed convection flow and heat transfer study in a rectangular cavity, Master's thesis, Indian Institute of Technology Guwahati, India, 2005.
[17] A. Dalal, M.K. Das, Laminar natural convection in an inclined complicated cavity with spatially variable wall temperature, Int. J. Heat Mass Transfer 48 (18) (2005) 3833–3854.
[18] A.B. Cortes, J.D. Miller, Numerical experiments with the lid driven cavity flow problem, Comput. Fluids 23 (1994) 1005–1027.
[19] K. Gustafson, K. Halasi, Vortex dynamics of cavity flows, J. Comput. Phys. 64 (1986) 279–319.
[20] O. Goyon, High-Reynolds number solutions of Navier–Stokes equations using incremental unknowns, Comput. Methods Appl. Mech. Eng. 130 (1996) 319–335.